Construction of a Test Field for Relative Gravimeters in a Cave With a Cold Atom Gravimeter

Bin Wu, Dianrong Li, Yin Zhou, Dong Zhu, Yingpeng Zhao, Zhongkun Qiao, Bing Cheng, Jingyu Niu, Xiaochun Guo, Xiaolong Wang, and Qiang Lin

***Abstract*—The Earth's gravity field is complex and variable. Performance evaluation of gravimeters requires gravity fields with well-known absolute gravity values. The aim of this study is to utilize an in-house developed cold atom gravimeter (CAG-E) in conjunction with CG-5 to establish a comprehensive test field consisting of 13 gravity datums at different altitudes. This absolute gravity field can be used for testing multiple relative gravimeters at the same time. The additional theoretical model calculations of this test field can provide a reference for gravity values at different heights, and a 3-D test field can be constructed in the future. In addition, a detailed performance evaluation of CAG-E was performed where the accuracy of the instrument repeatability was found to be 4.8 μGal. Finally, a correction of the geological density of the mountain was carried out using the absolute gravity values, and a minimum gravity difference residual of 0.9 μGal was obtained. These results verify the reliability of this test field for relative gravimeters.**

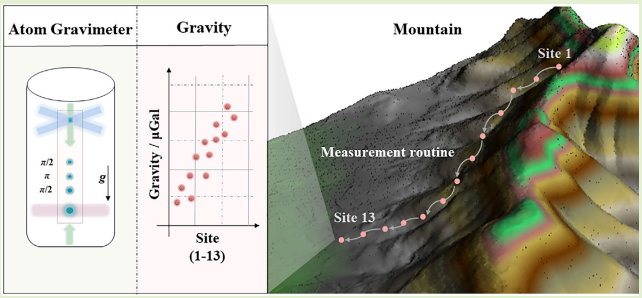

***Index Terms*— Cold atom gravimeters (CAGs-E), measurement accuracy, testing field for relative gravimeters.**

I. Introduction

THE advancement of various sensor technologies has significantly impacted biomedical applications [1], magnetic field measurements [2], [3], and precision measurements [4], [5], [6]. Gravity sensors, in particular, find utility in the field of gravity measurements. The precise measurements of gravity play a crucial role in several fields, including metrology, geophysics, and geodesy. Today, gravimeters are classified into two categories: relative and absolute gravimeters. The Scintrex CG-5 series and the superconducting gravimeters are examples of relative gravimeters, while the atom gravimeters belong to the absolute gravimeter category. Since the advent of atom interferometry in the laboratory in 1991 [7], atom gravimeters have been employed in numerous scientific studies, providing invaluable insights into areas such as the exact measurement of the fine structure constant (α) [8], the rotation angular velocity [9], gravitational waves [10], and gravity acceleration [11]. Among others, the exceptional capabilities of atom gravimeters have been well-established and documented in various works [12], [13], [14]. With the development of cold atom gravimeters (CAGs-E), they are not only used in laboratories, but in recent years have been gradually used in outdoor environments. For instance, a CAG can reach a sensitivity as good as 5.5 μGal at 1 s in the urban environment [15], a truck-borne system based on CAG was tested with an internal coincidence accuracy of 35.4 μGal and an external coincidence accuracy of 76.7 μGal [16].

Relative gravimeters are susceptible to various sources of errors, such as temperature fluctuations, tilt, long-term drift, and more [17], [18]. The Scintrex CG-3M and CG-5 must be calibrated based on gravity intervals [19], and multiple gravity measurements are often taken to mitigate drifts [20]. The Scintrex CG-5 relative gravimeters are generally calibrated by measuring on a baseline consisting of an absolute gravity

Manuscript received 11 January 2024; revised 1 February 2024; accepted 1 February 2024. Date of publication 16 February 2024; date of current version 2 April 2024. This work was supported in part by the National Key Research and Development Program of China under Grant 2023YFC2907000 and Grant 2017YFC0601602; in part by the National Natural Science Foundation of China under Grant 2022010202, Grant 61875175, Grant 61727821, Grant 11404286, and Grant 51905482; and in part by the Research Funds from the Ministry of Natural Resources of China under Grant DD20189831. The associate editor coordinating the review of this article and approving it for publication was Dr. Wensong Wang. *(Corresponding author: Yin Zhou.)*

The authors are with the Zhejiang Provincial Key Laboratory of Quantum Precision Measurement, College of Science, the Laboratory of Science and Technology on Marine Navigation and Control, China State Shipbuilding Corporation, and the Institute of Frontier and Cross-Science, Zhejiang University of Technology, Hangzhou 310023, China (e-mail: yinzhou@zjut.edu.cn; qiaozhongkun2021@zjut.edu.cn; qlin@zjut.edu.cn).

Digital Object Identifier 10.1109/JSEN.2024.3362371

datum to obtain an absolute gravity value or by determining the difference in the relative gravity segments between points. Usually, the linear and secondary drifts and scale factors are required to calibrate the relative gravimeters, especially in case multiple ones are used. The zero-drift rate of CG-5 is usually obtained as an instrumental parameter during the leveling calculation, in which the observation data are segmented according to the closed observation time of each line, and the leveling is performed by segment to calculate the zero-drift rate of each time segment. However, the zero-drift rate is affected by the observation environment and has higher requirements for the grid coefficient. The accuracy of the scale factor is related to its calibration method, which requires an absolute gravity point as a reference with the measured data. The prerequisite is the need for a good evaluation of the absolute gravimeters and correction for environmentally induced noise and systematic errors [21], [22]. Absolute gravimeters, such as the FG-5 series, are commonly used to calibrate relative gravimeters because of their estimated instrumental accuracy of about 2 μGal achieved through optical interferometry and an atom clock [23]. However, these absolute gravimeters have limitations, including susceptibility to mechanical wear and tear [24], [25], which restrict their suitability for continuous gravimetry, and a lower sampling rate compared to atom gravimeters. Therefore, absolute gravity values using the CAGs are reliable for providing comparisons and tests for the relative gravimeters. The calibration line established by Cheraghi et al. [26] covers a long distance of 2200 km and has been used for relative gravimeter calibrations for 12 years, where the gravity range is about 1200 mGal. The calibration coefficient of the relative gravimeters could be determined with an accuracy of about 40 ppm. However, repeated measurements of CG-3M and CG-5 showed that the gravity values of many stations have changed in time due to tectonic movements, land subsidence, and water depletion. For comparison, Onizawa [28] conduces the calibration line for the Scintrex CG-5 gravimeter with a gravity range of about 1400 mGal using the absolute gravity stations of the Japan Gravity Standardization. The scale factor can be corrected by introducing a gravity reading-dependent scale factor in this article and the scale factors varied by 1500 ppm in a range from 0.9991 to 1.0006. Such a large range is intended to cover the gravity range over which gravimeters normally operate so that the scale factors valid over the entire operating range can be calculated. However, such calibration lines are long and require a significant amount of time for measurements. In this article, we have established a test line, where the gravity range coverage is slightly less than 1.3 mGal. While the test line does not cover the entire gravity range of relative gravimeters, its shorter line allows for quicker measurements and yield more accurate relative gravity values. In addition, this test line can be used to test or compare the performance of relative gravimeters.

This article introduces a methodology for testing relative gravimeters, employing a CAG-E [29], [30], [31], [32], [33], [34] in conjunction with a CG-5 to establish an absolute gravity field in Laohe Mountain Cave, Hangzhou, China. The test line is short and situated within a tranquil cave, situated far away from human activities. This remote location ensures optimal testing performance, as it minimizes vibration noises and provides a stable measurement environment. Besides, a Polyhedral model is used to obtain not only the theoretical gravity values for each site but also the gravity gradient values on this line. Actually, the accurate modeling of the mountain could be helpful for providing an independent set of theoretical gravity values for the whole cave space for comparison, which may be useful for testing and comparisons of several relative gravimeters at the same time and location. Therefore, the application of CAG-E and mountain modeling in this study for the development of a test line presents distinct benefits in an academic context.

Fig. 1. CAG-E measurement system.

II. Data

A. Experimental Setup of CAG-E

Fig. 1 shows the CAG-E instrument with its three integral components: a gravity sensor, an optical system, and an electronic system, housed within two cabinets. In order to make the CAG-E perform well in caves, we have adopted a miniaturize vacuum sensor, a more compact and robust optical path with a stable support structure. The gravity sensor is surrounded by a magnetic field shield with a diameter of 52 cm and height of 55 cm, and the weight of gravity sensor is about 70 kg [31], [35]. With the 2-D and 3-D quartz vacuum chambers, an atomic loading rate of 8×10^9/s is achieved, enabling successful trapping of ^{87}Rb for gravity measurement [36]. The microwave antenna for atomic state selection is integrated above the 3-D Magneto-Optical Trap (3D-MOT) chamber [37], [38]. The detection region is under the 3D-MOT chamber, and a fluorescence collecting system is located at the same height. In the experiment, the optical system provided laser beams of different frequencies. The system features a compact and resilient optical path, minimizing reliance on spring structure and incorporating a

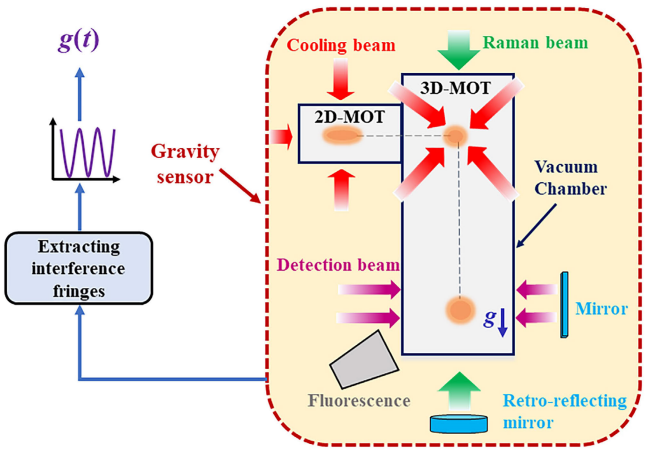

Fig. 2. Schematic of the CAG-E.

supplementary temperature control system, the stability of controlled temperature is less than 0.1 °C [16]. The electronic control systems are centralized in a 10 U control cabinet, weighing 90 kg and consuming 150 W of power, which consists of a data acquisition card, acousto-optic modulator (AOM) drivers [39], [40], magnetic field drivers, power supply module, frequency chain module [41], etc. Additionally, the CAG-E measurement system is equipped with an integrated tilt meter in the gravity sensor to calibrate its perpendicular position. The degrees of the inclinometer need to be calibrated prior to the measurement, which enables the adjustment of the μrad accuracy. The CAG-E was positioned in an arched cavern powered by an uninterruptible power supply (UPS) during the measurement period, and the surrounding environment's humidity was controlled using a dehumidifier. Upon leveling, the CAG-E initiates gravity data measurement and utilizes the computer for data acquisition and processing, which has a sampling rate of 2 Hz.

The schematic of CAG-E is depicted in Fig. 2. The ^{87}Rb atoms are loaded via the 2D-MOT and 3D-MOT and held in place by six laser beams. Upon switching off the magnetic field, the laser beams undergo a detuning process that imparts a polarization gradient to the rubidium atoms, reducing its temperature to be about 4 μK. Then the atoms drop freely due to gravity. The process from capturing atoms to releasing them is the preparation process of cold atoms, which ensures the coherence of atoms and lasts approximately 300 ms. After the atoms fall for a few milliseconds, through microwave state selection and Raman velocity selection, atoms with a narrow velocity distribution and guided to the $F = 2, m_F = 0$ state. Comprising three Raman pulses $\pi/2, \pi, \pi/2$ with a pulse duration of 10 μs and an interval of $T = 55$ ms, the sequence performs atom interferometry. Finally, a pair of counter-propagating detecting laser beams illuminates on the falling atoms. The fluorescence is collected by the fluorescence collecting system. We adopt a method of time of flight (TOF) to evaluate the number and the temperature of atoms. Utilizing a normalized detection method, the signal $P = P_0 + C\cos(\Delta\varphi)$ implies the correlation between the final interference phase $\Delta\varphi$ and the transition probability P, where P_0, C, and $\Delta\varphi$ signify the offset, fringe contrast, and the phase

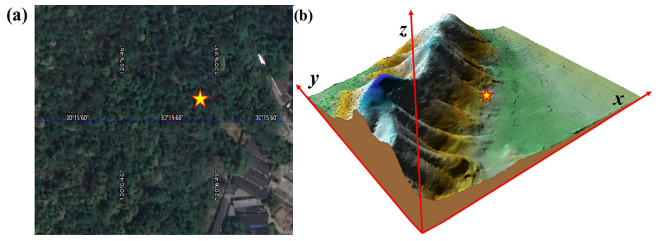

Fig. 3. Location of the test line. (a) Selection of measuring locations in satellite maps. (b) Three-dimensional terrain of the survey area, with the entrance to the cave marked by a five-pointed star.

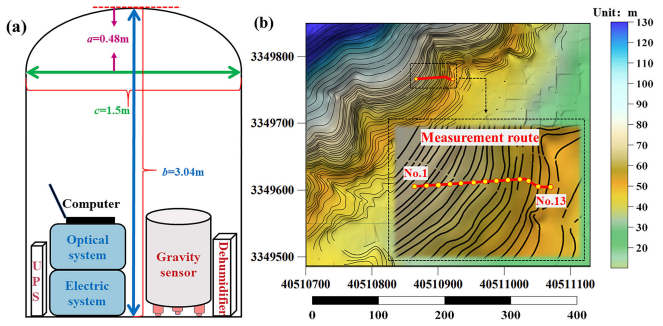

Fig. 4. Measurement devices and selection of the test line. (a) Schematic of CAG-E in the cave. (b) Contour map of the survey area's terrain (BJ54 coordinate system).

of interference fringes, respectively, $\Delta\varphi = (\vec{k}_{\text{eff}} \cdot \vec{g} - \alpha)T^2$, with $\vec{k}_{\text{eff}}$ denoting the effective wave vector of Raman beam, α being the chirp rate of the Raman pulse, and $\vec{g}$ being the gravitational acceleration. The fringe pattern, in turn, conveys the gravitational acceleration information, extracted by scanning α.

B. Selection of the Test Line

Embarking on a quest for accuracy, a remote and secluded cavity within the rugged Laohe Mountain, located in the heart of Hangzhou City in the province of Zhejiang, was chosen as the ideal site for conducting a gravity test field experiment. The pentagram in Fig. 3(a) and (b) denotes the entrance of the cave. In order to reduce the impact of human-generated vibrations, the site was chosen in a cave, and a route along the mountain served as the survey line. The width of cavern c is 1.5 m, and the maximum height between the ground and the top of the cave was 3.04 m, which is denoted by b. The height of the cave arch is 0.48 m, which is denoted by a in Fig. 4(a). The topographic calibration was established using 13 strategically placed measurement points, with an altitude difference of 2 m. Despite the uneven distribution of terrain, the measurement sites, spaced at intervals of 4.70 m apart (1–10) and 3.60, 5.40, and 5.00 m apart (11–13), respectively, as illustrated in Fig. 4(b), were chosen with utmost care. Additionally, in order to reduce the gravity values determined at the measurement height of the CAG-E to the ground or the measurement height of the relative gravimeters, it was deemed necessary to capture the gravity gradient information of the cave. In addition, the contribution of ground vibration noise from the cave to the gravimeter was assessed, and the gravity measurement sensitivity caused by the vibration

noises has been estimated to be 108.8 μGal/Hz$^{1/2}$ during the daytime and 72.1 μGal/Hz$^{1/2}$ at night, which means that the position is suitable for field measurements.

C. Absolute Gravity Measurements With CAG-E

We use CAG-E to conduct absolute gravity measurements sequentially from the deepest of the cave as the starting point and to the cave entrance as the endpoint. First, we perform tilt modulation experiments to find the true vertical direction of the gravity sensor, and the verticality of the gravity sensor can eventually be adjusted by a specific value of the inclinometer [42]. Then, each site is measured for a duration of 1 h, resulting in 7200 gravity values from which the final gravity value for the location is calculated. With the aim of determining the repeatability of the instrument, the measurement trajectory followed a closed-loop pattern, starting from site 1 and proceeding to site 13, then reversing back to site 1.

The accuracy of instrument repeatability σ of CAG-E was calculated using the following equation:

$$\sigma = \sqrt{\frac{1}{n}\sum_{n=1}^{n}\left[g_{n1} - \left(\frac{g_{n1}+g_{n2}}{2}\right)\right]^2} \tag{1}$$

where n is the number of measurement sites; g_{ni} $(i = 1, 2)$ denotes one of the two gravity measurement values at a specific site, n.

D. Relative Gravity Measurements With CG-5

For the relative gravity values, in addition to using CAG-E, we also utilized CG-5 as a comparative experiment. After leveling the CG-5, we record three readings during one setup, and the average of the three readings is used as the relative gravity values of this setup. The measurement sequence is from sites 1 to 13 and then back, a total of three round trips and six measurements for sites 2–12, 5 measurements for sites 1 and 4 measurements for site 13. The uncertainty of CG-5 is 10.7 μGal.

To further shed light on the gravity landscape of the 13 points under scrutiny, the authors leveraged the power of CG-5 relative gravimeters by carrying out the measurements of gravity gradients at these points, as depicted in Fig. 5(a). In this setup, the CG-5 instrument was strategically placed on a stand at four different heights, including these points on the ground, with each incrementing 50.7 cm from the previous level. At the ground level, the effective height of CG-5 is about 17.47 cm above the ground. The measurement approach is illustrated in Fig. 5(b), where the abscissa represents the level of the horizontal ground, and the ordinate signifies the height of the internal sensor of CG-5 from the ground. At each measuring point, CG-5 is positioned sequentially in numerical order at varying heights for measurement purposes.

However, the CG-5 is affected by the built-in spring, so drift correction is required. At first, we used the software of MATLAB to load the relative gravity values and time of CG-5 and extract them by measurement site serial numbers. The first site was used as the reference point in the experiment and a linear fitting was used to relate the relative gravity values over time. Thus, we can get the drift-corrected relative gravity values for each measurement site at different moments in time. Finally, we averaged the corrected relative values at different moments for each site as the relative gravity value for CG-5 at that site.

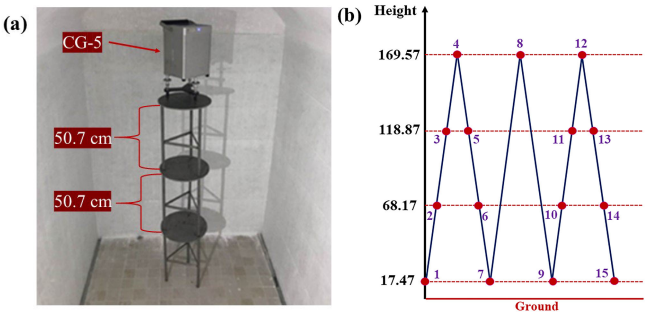

Fig. 5. Measurement process of gravity gradient in the cave. (a) Illustrating the measurement of gravity gradient using CG-5. (b) Way CG-5 measures gravity gradients.

III. Modeling

Firstly, a high accuracy digital elevation model (DEM) model is employed for the purpose of engineering a topographical depiction of the measurement region, which is resolved with a resolution of 1 m. Subsequently, using the uniform Polyhedron model, based on the coordinate data and surrounding terrain data, the relative gravity values and gravity gradient values of the measuring points are obtained. The mountain modeling with measurement points is shown in Fig. 6. The x–y–z coordinates are the geological length, width, and height of the cave model in the BJ54 coordinate system.

In the process of calculating the relative gravity values with the Polyhedron model, the volumetric integration present in the 3-D potential field undergoes a transformation into surface area integration, which is presented using a planar triangle to accommodate a curved surface. The gravitational impact provoked by the polyhedron is illustrated by the following equation:

$$g_{\text{poly}} = G\rho \iiint_V \frac{\partial}{\partial Z}\left(\frac{1}{r}\right) dv \tag{2}$$

where G represents the universalgravitational constant, ρ stands for the average density of the polyhedron, r represents the distance between the calculation point and the volume element dv, while z denotes the vertical component of r. Utilizing Gauss' divergence theorem, this is then transformed into surface area integration, where the sum of multiple triangular surfaces S_j $(j = 1, 2, \ldots, m)$ can be expressed as [43]

$$g = G\rho \sum_{j=1}^{m}\left[\cos(n_j, z) \iint_{S_j} \frac{1}{r} ds\right] \tag{3}$$

where $\cos(n_j, z)$ is a constant that defines the outward normal of the surface with respect to the z-axis. Finally, a new Cartesian coordinate system is defined, where the z-direction coincides with the outward normal direction of S_j, and the surface area integration is transformed into a line integral to obtain the results.

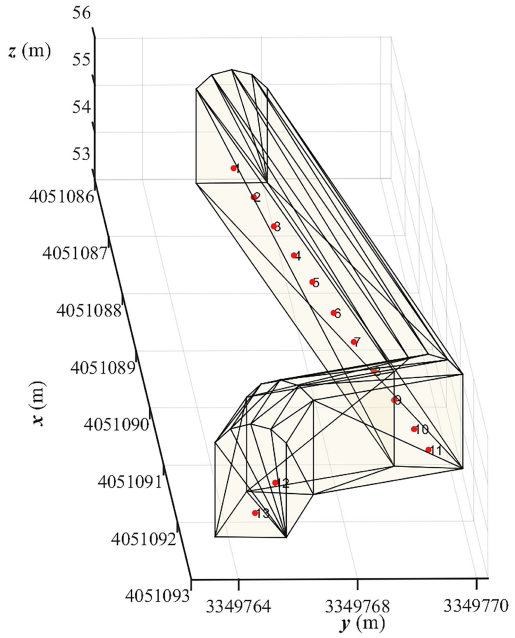

Fig. 6. Simulation of mountain shape with a Polyhedral model.

It is worth noting that these values need to be juxtaposed with the fluctuations in the gravity segment difference values of CAG-E and CG-5 to verify the credibility of the Polyhedral forward modeling and parameter settings. Since the two instruments have disparate probe measurement heights, in order to garner precise absolute gravity values at the ground level, gravity gradient measurements are undertaken with CG-5 before the gravity data of the two sets of measurements can be rectified to a similar height at the same measuring site.

IV. Results

A. Absolute Gravity Values Measured by CAG-E

Atom interference fringes are obtained by varying the chirp rate α. Interference fringes are measured with different intervals T. These fringes have a common constant chirp rate, α_0, that corresponds to the valley of dark fringes. α_0 contains information on the absolute gravity values, and the gravity value is calculated by data processing. For ease of representation and comparison, we subtract the constant g_0 from the values corrected for systematic error and noise assessment, which is used to denote Δg. The uncertainty of CAG-E is typically 8.9 μGal. The Δg values and uncertainties are shown in Fig. 7.

At the beginning of the measurement, the systematic errors and the measurement noises have been estimated and will be checked frequently during the measurements. The effects of laser frequency, RF phase shift, two-photon light shift, Coriolis force, and gravity gradient were mainly evaluated for systematic errors. The Type A uncertainties of 3.4 μGal is obtained for the measurements, and the Type B uncertainty is 8.2 μGal. Thus, the typical uncertainty of the CAG-E is 8.9 μGal.

B. Instrument Repeatability of the CAG-E

The result of the repeatability of CAG-E is shown in Fig. 8. In Fig. 8(a) the black squares indicate fixed-site measurements

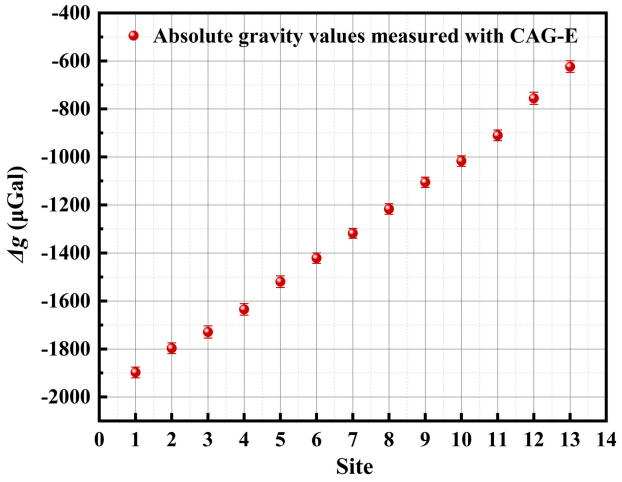

Fig. 7. Gravity values Δg of the measurement sites 1–13 reference to a constant absolute gravity value of g_0.

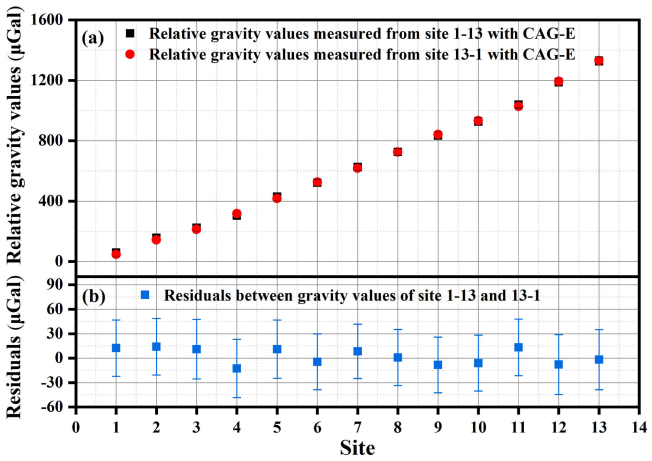

Fig. 8. Instrument repeatability of CAG-E. (a) Gravity values measured by CAG-E. (b) Residuals between two measurements.

from 1 to 13, while the red dots denote the measurements made from 13 to 1. To aid visualization, each measurement site number is included. The residuals of the two measurements are shown in Fig. 8(b). Notably, the values after subtracting an identical constant value of g_0 at each site are shown in Table I. The accuracy of instrument repeatability is obtained with (1) as 4.8 μGal.

C. Comparison Between Relative Values

In addition, the relative gravity values obtained with CG-5 were compared with CAG-E, as shown in Fig. 9. Fig. 9(a) represents the relative gravity difference between the nth ($n = 2, 3, \ldots, 13$) site and the 1st site, which considers site 1 as a reference. Fig. 9(b) represents the residuals of the CG-5 and CAG-E gravity values differences. The residuals of the relative gravity values of CG-5 and CAG-E range from -30.2 to 7.2 μGal and the average of residuals is -7.9 μGal. The values and residuals of relative gravity are as shown in Table II, where the CAG-E values in Table II are the average values for each site from Table I and are corrected to the height of the CG-5 measurements using the gravity gradients.

TABLE I
GRAVITY VALUES AND THE RESIDUAL VALUES OF 13 MEASURED SITES FOR TWO ABSOLUTE MEASUREMENTS WITH CAG-E

Number	Absolute gravity values from site 1-13 (μGal)	Absolute gravity values from site 13-1 (μGal)	Residuals of two absolute measurements with CAG-E (μGal)
1	59.91	47.57	12.34
2	157.44	143.33	14.11
3	225.05	213.94	11.11
4	305.84	318.39	-12.56
5	429.95	418.80	11.14
6	522.30	526.73	-4.43
7	626.16	617.75	8.41
8	726.05	725.24	0.81
9	833.57	841.98	-8.41
10	927.30	933.31	-6.07
11	1039.96	1026.70	13.25
12	1186.98	1194.83	-7.86
13	1328.53	1330.28	-1.75

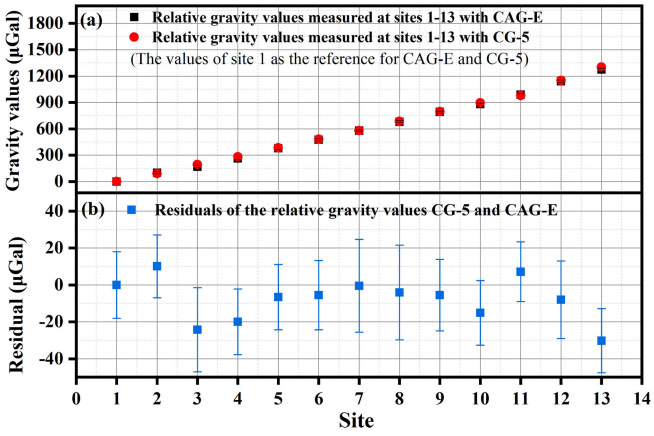

Fig. 9. Relative gravity values of sites 2nd–13th with reference to site 1st with CG-5 and CAG-E. (a) Values in gravity measurements between the 2nd–13th sites and the first site was measured utilizing CAG-E and CG-5, respectively. (b) Residuals of readings of two instruments.

TABLE II
RELATIVE GRAVITY VALUES OF SITES 2nd–13th WITH REFERENCE TO SITE 1st WITH CG-5 AND CAG-E

Number	Relative gravity values with reference to site 1 with CG-5 (μGal)	Relative gravity values with reference to site 1 with CAG-E (μGal)	Residuals of relative gravity values between CG-5 and CAG-E (μGal)
1	0	0	0
2	90.9	101	10.1
3	193	168.8	-24.2
4	282.8	262.8	-20
5	384.8	378.2	-6.6
6	482.1	476.5	-5.6
7	579.7	579.2	-0.5
8	684.8	680.7	-4.1
9	797.5	792	-5.5
10	895.6	880.5	-15.1
11	980.5	987.7	7.2
12	1150.2	1142.1	-8.1
13	1304.1	1273.9	-30.2

In addition, this article provides an independent set of theoretical values of relative gravity for comparison. The relative gravity values with reference to site 1 calculated

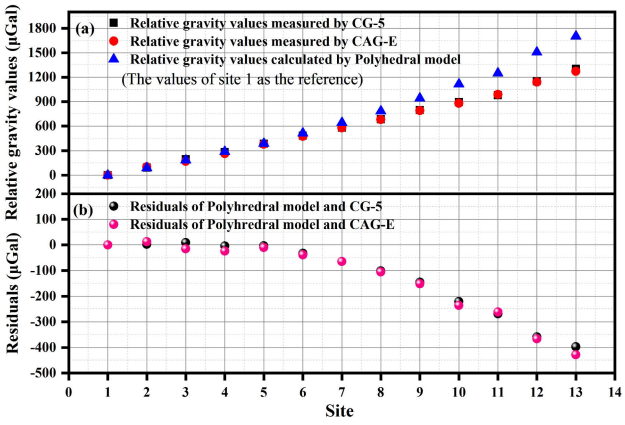

Fig. 10. Relative gravity values of the modified Polyhedral model and the actual gravity values measured with CG-5 and CAG-E. (a) Comparison of relative gravity values obtained with CAG-E, CG-5, and Polyhedral model, which between the 2nd through 13th sites and the first site. (b) Residuals of readings of three comparisons.

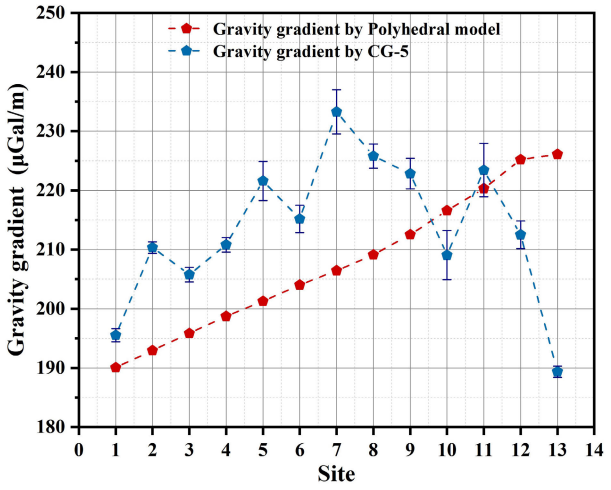

Fig. 11. Comparison of gravity gradients obtained using CG-5 and Polyhedral model (red hexagon represents theoretical gravity gradient value by Polyhedral model, while blue pentagon indicates gravity gradient value measured by CG-5).

with the Polyhedral model are compared with CAG-E and CG-5 as shown in Fig. 10(a). The blue triangles signify the relative gravity value differences obtained by applying the Polyhedral model, while the gray squares and the red dots represent the value differences acquired through the utilization of CG-5 and CAG-E. The black dots represent the residuals between the modeling value differences and CG-5 measured value differences, and the residuals span a range from 2.4 to 397.7 μGal. The pink dots represent the residuals between the theoretical calculation value differences and the CAG-E measurement value differences, with differences ranging from 12.5 to 427.9 μGal, which can be seen in Fig. 10(b), with an average rock density of 2.6×10^3 kg/m^3. The modeled values and the relative gravity differences measured by CAG-E do not match well. The explanation could be the density distribution of mountains has large uncertainty and inhomogeneity, in the case of unknown mountain density distribution.

The resulting distribution of the measured gradient values is depicted in Fig. 11, revealing that the gradient values in the

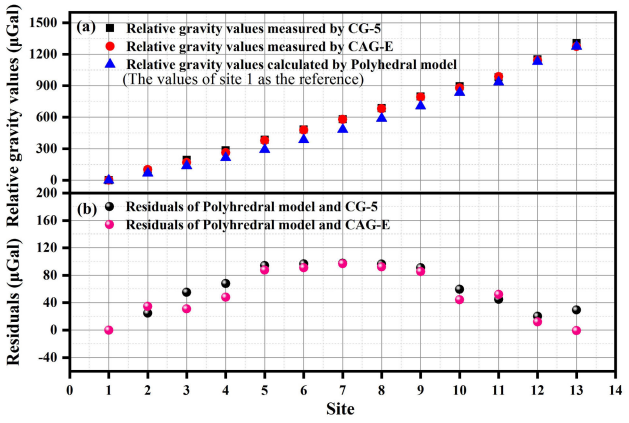

Fig. 12. Relative gravity values of the modified Polyhedral model and the actual gravity values measured with CG-5 and CAG-E. (a) Comparison of relative gravity values obtained with CAG-E, CG-5, and the Polyhedral model, between the 2nd through 13th sites and the 1st site. (b) Residuals of readings of comparisons.

center of the cave exhibit a greater magnitude compared to the two extremities of the cave. This observation may be the result of a gravity anomaly brought about by the inhomogeneous density structure of the area. Further to the comparison between the Polyhedral model and CG-5 measurements, the predominant causes for the dissimilarities observed between the theoretical and experimental outcomes are as follows: measurement errors associated with the instruments, inadequate accuracy in the elevation data of the measurement zone, the nonhomogeneous density of the encasing rocks around the measurement points, and the indeterminable authentic density. The forward data incurred inaccuracies as a result of the Polyhedral model's supposition of uniform density distribution across the entire mass of the terrain. Moreover, the forward process disregarded the impact of the cave itself. Subsequently, the accuracy of the gravity gradient can be further improved by adding more measurement points, and the effect of uneven density distribution on the gravity gradient can be assessed by drilling holes around the mountain to measure the density of the rock at different depths.

Based on the residuals of the Polyhedral model and the CAG-E, we corrected the density of the mountain and got the results as shown in Fig. 12, using the corrected density. The calculated values with the theoretical model are in good agreement with that of CAG-E. The minimum residual error is 0.9 μGal and the maximum is 96.9 μGal.

V. Conclusion

With the purpose of establishing a comprehensive absolute gravity testing field for relative gravimeters, this study utilizes the CAG-E for conducting absolute gravity measurements at 13 distinct sites. A meticulous evaluation of the CAG-E was performed, including the determination of the instrument repeatability, which was determined to be 4.8 μGal. Furthermore, the theoretical models for relative gravity value differences were employed and compared to the CAG-E gravity value differences, resulting in an agreement that varied between a maximum residual of 427.9 μGal to a minimum of 12.5 μGal, while the geological density is 2.6×10^3 kg/m^3. The density of the mountain was corrected with the absolute gravity values measured with CAG-E leading to congruent results, with a residual range from 0.9 to 96.9 μGal. Despite these findings that suggest the absolute gravity field provides robust data for the testing and comparisons of relative gravimeters, there is still scope for improvement.

The theoretical model adapted in this article uses a constant density, but the deep geological distribution is uneven in the actual situation. Therefore, it is necessary to evaluate the impact on different geological layers for the theoretical model in the future. For example, boreholes can be selected at different locations around the mountain to measure the geological density at different depths and optimize the theoretical algorithms. In addition, the CAG-E used in the measurement can be improved in terms of sensitivity by increasing the length of the interference zone.

Acknowledgment

The authors are grateful to other colleagues for their help during the period of experimental measurement.

References

[1] W. Wang et al., "MRC-based double figure-of-eight coil sensor system with triple-mode operation capability for biomedical applications," *IEEE Sensors J.*, vol. 21, no. 13, pp. 14491–14502, Jul. 2021.

[2] W. Wang et al., "Novel coil transducer induced thermoacoustic detection of rail internal defects towards intelligent processing," *IEEE Trans. Ind. Electron.*, vol. 71, no. 2, pp. 2100–2111, Feb. 2024.

[3] W. Wang et al., "Analysis and design of coil-based electromagnetic-induced thermoacoustic for rail internal-flaw inspection," *IEEE Trans. Intell. Transp. Syst.*, vol. 20, no. 7, pp. 2691–2702, Jul. 2019.

[4] B. Wu et al., "A simplified laser system for atom interferometry based on a free-space EOM," *Photonics*, vol. 9, no. 5, p. 301, Apr. 2022.

[5] B. Wu et al., "Marine absolute gravity field surveys based on cold atomic gravimeter," *IEEE Sensors J.*, vol. 23, no. 20, pp. 24292–24299, Oct. 2023.

[6] Z.-K. Qiao et al., "Error analysis and filtering methods for absolute ocean gravity data," *IEEE Sensors J.*, vol. 23, no. 13, pp. 14346–14355, Jul. 2023.

[7] M. Kasevich and S. Chu, "Atomic interferometry using stimulated Raman transitions," *Phys. Rev. Lett.*, vol. 67, no. 2, pp. 181–184, Jul. 1991.

[8] R. H. Parker, C. Yu, W. Zhong, B. Estey, and H. Müller, "Measurement of the fine-structure constant as a test of the standard model," *Science*, vol. 360, no. 6385, pp. 191–195, Apr. 2018.

[9] I. Dutta et al., "Continuous cold-atom inertial sensor with 1 nrad/sec rotation stability," *Phys. Rev. Lett.*, vol. 116, no. 18, May 2016, Art. no. 183003.

[10] J. Su, Q. Wang, Q. Wang, and P. Jetzer, "Low-frequency gravitational wave detection via double optical clocks in space," *Classical Quantum Gravity*, vol. 35, no. 8, Apr. 2018, Art. no. 085010.

[11] G. Rosi, L. Cacciapuoti, F. Sorrentino, M. Menchetti, M. Prevedelli, and G. M. Tino, "Measurement of the gravity-field curvature by atom interferometry," *Phys. Rev. Lett.*, vol. 114, no. 1, Jan. 2015, Art. no. 013001.

[12] Y. Bidel et al., "Absolute marine gravimetry with matter-wave interferometry," *Nature Commun.*, vol. 9, no. 1, p. 627, Feb. 2018.

[13] V. Ménoret et al., "Gravity measurements below 10^{-9}g with a transportable absolute quantum gravimeter," *Sci. Rep.*, vol. 8, no. 1, p. 12300, Aug. 2018.

[14] A. Louchet-Chauvet et al., "Comparison of 3 absolute gravimeters based on different methods for the e-MASS project," *IEEE Trans. Instrum. Meas.*, vol. 60, no. 7, pp. 2527–2532, Jul. 2011.

[15] S. Merlet et al., "Operating an atom interferometer beyond its linear range," *Metrologia*, vol. 46, no. 1, pp. 87–94, Feb. 2009.

[16] H. Wang et al., "A truck-borne system based on cold atom gravimeter for measuring the absolute gravity in the field," *Sensors*, vol. 22, no. 16, p. 6172, Aug. 2022.

[17] B. Hábel, J. Janák, J. Papč o, and M. Val'ko, "Impact of environmental phenomena on continuous relative gravity measurements performed in urban area," *Studia Geophysica et Geodaetica*, vol. 64, no. 3, pp. 330–348, Jul. 2020.

[18] P. Gettings, D. S. Chapman, and R. Allis, "Techniques, analysis, and noise in a salt lake valley 4D gravity experiment," *Geophysics*, vol. 73, no. 6, pp. 71–82, Nov. 2008.

[19] Q. Zheng, D. Liu, L. Wang, J. Huang, and Q. Wang, "Bayesian estimation of scale factor for CG-5 relative gravimeter," *IOP Conf. Ser., Earth Environ. Sci.*, vol. 734, no. 1, Apr. 2021, Art. no. 012037.

[20] D. Boddice, P. Atkins, A. Rodgers, N. Metje, Y. Goncharenko, and D. Chapman, "A novel approach to reduce environmental noise in microgravity measurements using a scintrex CG5," *J. Appl. Geophys.*, vol. 152, pp. 221–235, May 2018.

[21] R. Karcher, F. P. Dos Santos, and S. Merlet, "Impact of direct-digital-synthesizer finite resolution on atom gravimeters," *Phys. Rev. A, Gen. Phys.*, vol. 101, no. 4, Apr. 2020, Art. no. 043622.

[22] A. Gauguet et al., "Off-resonant Raman transition impact in an atom interferometer," *Phys. Rev. A, Gen. Phys.*, vol. 78, no. 4, Oct. 2008, Art. no. 043615.

[23] G. S. Sasagawa, F. Klopping, T. M. Niebauer, J. E. Faller, and R. L. Hilt, "Intracomparison tests of the FG5 absolute gravity meters," *Geophys. Res. Lett.*, vol. 22, no. 4, pp. 461–464, Feb. 1995.

[24] T. M. Niebauer, G. S. Sasagawa, J. E. Faller, R. Hilt, and F. Klopping, "A new generation of absolute gravimeters," *Metrologia*, vol. 32, no. 3, pp. 159–180, Jan. 1995.

[25] D. Crossley, J. Hinderer, and U. Riccardi, "The measurement of surface gravity," *Rep. Prog. Phys.*, vol. 76, no. 4, Apr. 2013, Art. no. 046101.

[26] H. Cheraghi et al., "Stability of the calibration of scintrex relative gravimeters as inferred from 12 years of measurements on a large amplitude calibration line in Iran," *Pure Appl. Geophys.*, vol. 177, no. 2, pp. 991–1004, Feb. 2020.

[27] B. Richter, H. Wilmes, and I. Nowak, "The Frankfurt calibration system for relative gravimeters," *Metrologia*, vol. 32, no. 3, pp. 217–223, Jan. 1995.

[28] S. Onizawa, "Apparent calibration shift of the scintrex CG-5 gravimeter caused by reading-dependent scale factor and instrumental drift," *J. Geodesy*, vol. 93, no. 9, pp. 1335–1345, Sep. 2019.

[29] B. Cheng et al., "Experiment on dynamic absolute gravity measurement based on cold atom gravimeter," *Acta Phys. Sinica*, vol. 71, no. 2, 2022, Art. no. 026701.

[30] B. Wu et al., "Influence of Raman laser sidebands effect on the measurement accuracy of cold atom gravimeter," *Acta Phys. Sinica*, vol. 68, no. 19, 2019, Art. no. 194205.

[31] Z. Fu et al., "A new type of compact gravimeter for long-term absolute gravity monitoring," *Metrologia*, vol. 56, no. 2, Apr. 2019, Art. no. 025001.

[32] C. Bing et al., "Absolute gravity measurement based on atomic gravimeter under mooring state of a ship," *Acta Phys. Sinica*, vol. 70, no. 4, 2021, Art. no. 040304.

[33] B. Wu et al., "Dependence of the sensitivity on the orientation for a free-fall atom gravimeter," *Opt. Exp.*, vol. 27, no. 8, pp. 11252–11263, Apr. 2019.

[34] Y. Zhou et al., "Active vibration isolation system based on the LADRC algorithm for atom interferometry," *Appl. Opt.*, vol. 59, no. 11, pp. 3487–3493, 2020.

[35] B. Wu et al., "Static measurement of absolute gravity in truck based on atomic gravimeter," *Acta Phys. Sinica*, vol. 69, no. 6, 2020, Art. no. 060302.

[36] K. Weng, B. Wu, J. Lin, Y. Zhou, B. Cheng, and Q. Lin, "Compact magneto-optical trap with a quartz vacuum chamber for miniature gravimeters," *J. Opt. Soc. Amer. B, Opt. Phys.*, vol. 37, no. 6, p. 1637, 2020.

[37] W. Wang, S. Yang, Z. Fang, Q. Sun, Y. Chen, and Y. Zheng, "Compact dual-polarized wideband antenna with dual-/single-band shifting for microbase station applications," *IEEE Trans. Antennas Propag.*, vol. 69, no. 11, pp. 7323–7332, Nov. 2021.

[38] W. Wang, Y. Chen, S. Yang, A. Chan, Y. Wang, and Q. Cao, "Design and experiment of wireless power transfer systems via electromagnetic field near-zone region," *Int. J. Electron.*, vol. 103, no. 10, pp. 1736–1747, Oct. 2016.

[39] W. Wang, Q. Cao, C. Yang, Y. Wang, and Y. Chen, "Design of dual-bandpass filters using stepped-impedance circular ring resonator," *Electron. Lett.*, vol. 51, no. 25, pp. 2117–2119, Dec. 2015.

[40] W. Wang, Y. Zheng, and Q. Cao, "A four-way broadband filtering power divider with improved matching network for X-band application," *Microw. Opt. Technol. Lett.*, vol. 61, no. 9, pp. 2155–2160, Sep. 2019.

[41] W. Wang, C. Yang, Q. Cao, and Y. Chen, "Dual-band BPF design using Asir structures with a dumbbell-shaped notch," *Microw. Opt. Technol. Lett.*, vol. 58, no. 3, pp. 532–535, Mar. 2016.

[42] Z. F. Z. Fu, Q. W. Q. Wang, Z. W. Z. Wang, B. W. B. Wu, B. C. B. Cheng, and Q. L. Q. Lin, "Participation in the absolute gravity comparison with a compact cold atom gravimeter," *Chin. Opt. Lett.*, vol. 17, no. 1, 2019, Art. no. 011204.

[43] X. Li and M. Chouteau, "Three-dimensional gravity modeling in all space," *Surv. Geophys.*, vol. 19, no. 4, pp. 339–368, 1998.

Bin Wu received the Ph.D. degree in optics from the Department of Physics, Zhejiang University, Hangzhou, China, in 2014.

In 2012, he went to LNESYRTE, Paris, France, on a joint training program. After the Ph.D. degree, he joined the College of Science, Zhejiang University of Technology, Hangzhou, where he is currently an Associate Professor, working on quantum precision measurement science and technology, quantum optics, cold atomic physics, and atomic interferometry.

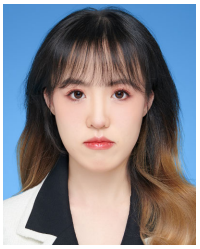

Dianrong Li is pursuing the Ph.D. degree with the College of Science, Zhejiang University of Technology, Hangzhou, China.

Her research interests include dynamic cold atom gravity measurement and quantum optics.

Yin Zhou received the B.S. degree in microelectronics from Jilin University, Changchun, China, in 2014, and the Ph.D. degree in control science and engineering from the Zhejiang University of Technology, Hangzhou, China, in 2020.

He is currently a Postdoctoral Researcher with the Zhejiang University of Technology. His research interests include atom interferometry and precision absolute gravity measurement.

Dong Zhu received the Ph.D. degree from the College of Information Engineering, Zhejiang University of Technology, Hangzhou, China, in 2022.

He is a Postdoctoral Researcher with the College of Science, Zhejiang University of Technology. His research interests include cold atom gravimeter, dynamic absolute gravimeter, and data processing.

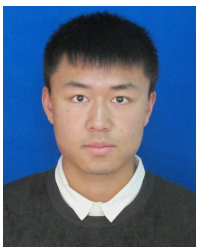

Yingpeng Zhao is pursuing the Ph.D. degree with the School of Science, Zhejiang University of Technology, Hangzhou, China.

His research interests include the fields of cold atom interferometry, quantum precision measurement, and diffraction measurement.

Zhongkun Qiao received the Ph.D. degree from the College of Earth Exploration Science and Technology, Jilin University, Changchun, China, in 2021.

He is a Lecturer with the Institute for Frontiers and Interdisciplinary Sciences, Zhejiang University of Technology, Hangzhou, China. His research interests include research and application of geophysical exploration technology in aviation and ocean.

Bing Cheng received the Ph.D. degree in optics from Zhejiang University, Hangzhou, China, in 2013, and the Ph.D. degree from the Paris Observatory, Paris, France, in 2016.

His research interests include technical areas including laser transmission, laser frequency control, laser cooling principles, atom laser interactions, and atomic interference.

Jingyu Niu is pursuing the master's degree with the School of Science, Zhejiang University of Technology, Hangzhou, China.

His research interests include quantum precision measurement.

Xiaochun Guo is pursuing the master's degree with the School of Science, Zhejiang University of Technology, Hangzhou, China.

His research interests include quantum precision measurement and ultrahigh vacuum environment.

Xiaolong Wang received the Ph.D. degree in optics from the Department of Physics, Zhejiang University, Hangzhou, China, in 2011, and the Ph.D. degree in physics from the Paris Observatory, Paris, France, in 2011.

His research interests include atom interferometry, spectroscopy, spectroscopic instruments, and optics and laser physics.

Qiang Lin received the Ph.D. degree in science from Zhejiang University, Hangzhou, China, in 2003.

He has long been engaged in the research of quantum precision measurement, quantum optics, and laser physics, including developing high-precision quantum gravimeter and quantum magnetometer and their applications.

Dr. Lin was a recipient of the National Natural Science Foundation of China Distinguished Youth Fund and the German Humboldt Fund.